PHYSICAL REVIEW FLUIDS **8**, 064003 (2023)

Role of odd viscosity on falling films over compliant substrates

Souradip Chattopadhyay,[1,*] Akshay S. Desai,[2,†]
Amar K. Gaonkar,[2,‡] and Anandamoy Mukhopadhyay[3,§]
[1]*Department of Mathematics, North Carolina State University, Raleigh, North Carolina 27695, USA*
[2]*Department of Mechanical, Materials and Aerospace Engineering, IIT Dharwad, Karnataka 580011, India*
[3]*Department of Mathematics, Vivekananda Mahavidyalaya (The University of Burdwan), West Bengal 713103, India*

(Received 31 October 2022; accepted 9 May 2023; published 16 June 2023)

We study the behavior of a thin liquid film flowing over a compliant substrate that is thin enough. The breakdown of time-reversal symmetry includes the odd component of the Cauchy stress tensor, resulting in some significant effects that were not previously explored. We utilize the long-wave theory to obtain equations coupling the thickness of the film and the compliant substrate. These equations consider inertia, damping effects, wall tension, and odd viscosity. Through linear stability analysis, we establish that the compliant substrate destabilizes the system while odd viscosity significantly stabilizes. We also apply a weakly nonlinear approach to explore the system's dynamics. The coupled long-wave equations lead to the derivation of the Kuramoto-Sivashinsky equation. Notably, incorporating the odd viscosity tensor component can avert chaotic behavior in compliant substrates within the weakly nonlinear limit. Numerical simulations reveal that the odd viscosity produces remarkable effects on substrate deflection. Furthermore, we demonstrate the consistency of the linear and weakly nonlinear theories with numerical results by performing a numerical investigation of the coupled long-wave equations.

DOI: 10.1103/PhysRevFluids.8.064003

I. INTRODUCTION

Studying thin liquid film flow down an inclined plane is a fascinating research field with diverse industrial applications. These applications ranged from thin coating processes in various industries and lubricated pipelining to the manufacturing of photographic plates. A thin liquid sheet must be applied evenly onto the substrate in the coating process. It is essential to suppress surface waves for manufacturing products with a smooth and glossy texture like photographic membranes. Thus, a comprehensive theoretical understanding of the behavior of thin film flow is vital for the design and improvement of coating technology.

A considerable amount of research has been devoted to analyzing the stability and dynamics of thin film flows on a rigid substrate, resulting in an extensive body of literature. For a thorough review of this literature, Refs. [1–4] provides an excellent source. A compliant substrate, commonly made of thin and heat-resistant polymers like polyimide and polyethylene terephthalate (PET), is a readily deformable material. During deformation at any given time t, the substrate can be mathematically represented as $z = f(x(S,t), y(S,t))$, where x and y are functions of arc length S and time t and

*schatto5@ncsu.edu
†akshay.desai.20@iitdh.ac.in
‡amar.gaonkar@iitdh.ac.in
§Corresponding author: anandamoymukhopadhyay@vmbdn.ac.in

(x, y, z) denotes the spatial coordinates of a point on the substrate. The fundamental structural difference between a compliant substrate and a rigid substrate is that, for a compliant substrate, a point's position depends on both time t and arc length S, whereas for a rigid substrate, the position depends only on the spatial coordinates. Fluid-compliant material interactions play a significant role in many scenarios, such as the wrinkling of thin sheets at fluid interfaces [5], the suppression of fingering instability with elastic membranes [6], and wrapping liquid droplets with elastic sheets [7]. In 2020, Nikravesh *et al.* [8] studied the instabilities of thin films on a compliant substrate, with a primary emphasis on developing a finite-element modeling approach for simulating wrinkle formation. Halpern and Grotberg's research [9,10] investigated the interaction between compliant substrates and thin liquid films. Their model provided insights into the mechanism behind airway collapse in the lungs and highlighted the impact of pulmonary surfactants in this scenario. Matar *et al.* [11] explored the stability and dynamics of thin liquid films on a flexible substrate and concluded that wall flexibility promotes flow instability. Sisoev *et al.* [12] then expanded on Matar *et al.*'s study [11] and delved into the nonlinear traveling wave solution. Howell *et al.* [13] analyzed the impact of a flexible substrate on the flow of a thin liquid film using the lubrication approximation framework. Another study conducted by Chao and Ding [14] examined the dynamics of a thin liquid film over a compliant substrate subjected to wall heating and found that the heating affects both the substrate and the thin liquid film. Alexander *et al.* [15] researched the linear stability of a thin liquid film flowing along a flexible wall inclined at an angle. Their study involved the use of an Orr-Sommerfeld-type boundary value problem. In a subsequent study, Samanta [16] expanded on the work of Alexander *et al.* [15] by including an insoluble surfactant on the surface of the liquid and imposing an external streamwise shear stress on the fluid surface. To obtain a comprehensive understanding of various compliant models, it is recommended to refer to the study by Alexander *et al.* [15].

In a viscous fluid that maintains time-reversal symmetry, the stress tensor is symmetric. However, if this symmetry is broken, then the viscosity tensor splits into even (symmetric) and odd (antisymmetric) parts, as demonstrated by Avron [17]. The dissipative effect is described by the symmetric part of the viscosity tensor, while the odd viscosity contributes to a nondissipative effect. Examples of odd viscosity include three-dimensional magnetized polyatomic gases such as N_2, CO, or CH_4, a two-dimensional fluid of electrons in graphene under a magnetic field, and a two-dimensional fluid containing small cubes with a permanent magnetic dipole moment in a colloidal suspension under a rotating magnetic field [18–21]. Avron [17] showed that time-reversal symmetry can naturally break in systems such as superfluid He^3 or in the presence of an external magnetic field (as in two-dimensional quantum Hall fluid) or due to rotation. Most studies on falling film instability have overlooked the odd part of the viscosity tensor. However, in recent years, researchers have begun to explore the impact of odd viscosity in various contexts, such as in chiral active fluids [22], incompressible fluids [23,24], swimming strategies [25], electric fields [26,27], electromagnetic fields [28], Rayleigh-Taylor instability [29], vertical moving plates [30], and others. Kirkinis and Andreev [31] investigated the effect of odd viscosity on a thin liquid film flow in the presence of thermocapillarity and broken time-reversal symmetry. They demonstrated that considering the odd viscosity coefficient could suppress surface waves induced by the thermocapillary effect. Monteiro and Ganeshan [32] investigated the impact of odd viscosity on shallow water dynamics. They found that within the Korteweg–de Vries dynamics, there exist two parity-breaking regimes—strong (with high odd viscosity) and weak (with low odd viscosity). Doak *et al.* [33] analyzed the impact of vertical odd viscosity on weakly and strongly nonlinear waves in three-dimensional nonlinear shallow water waves. They observed several striking effects of the vertical odd viscosity. Chattopadhyay [34] explored the effects of odd viscosity on the stability of a thin liquid film flowing along a uniformly heated inclined plane, taking into account variations in liquid surface tension and density due to temperature changes. The study showed that both the odd viscosity and the density change rate with temperature can stabilize surface instability. Additionally, Samanta [35] investigated the influence of odd viscosity on thin liquid films and found that the odd viscosity coefficient can weaken both surface and shear instabilities. Desai *et al.* [36] have recently investigated the behavior of a thin liquid film flowing on an inclined plane in the moderate Reynolds number regime under the influence of an imposed shear stress, with the time-reversal symmetry broken. Their study reveals that uphill shear tends to stabilize the flow, while downhill shear exacerbates the instability. However, the presence of odd viscosity can reduce this instability.

The present study is motivated by practical reasons for considering a compliant substrate that is extremely thin, rather than a rigid inclined substrate. There are several instances where such a scenario is applicable. For instance, in medical biology, administering liquids and surfactants into the pulmonary airways during surfactant replacement therapy, partial liquid ventilation, and drug delivery is a common practice [37]. Similarly, in human physiology, blood flows through the heart and lungs, which are flexible substrates. The rate and rhythm of the heartbeat are maintained through electric impulses that cause the heart muscle to contract and relax [38]. Moreover, rubber-coated rollers are used in industries to ensure uniform mix transfer and minimum wear during flexographic printing [39]. Additionally, blood flow in veins and arteries contains soft and flexible cells, which cause the bounding surface to deform when a biological flow system passes through it. These practical examples of flow systems have motivated us to study the effect of a compliant or flexible substrate on the stability and dynamics of the flow.

Existing literature suggests that when the time-reversal symmetry of a liquid is broken in thin film flows over a rigid or moving substrate, the inclusion of the odd part of the viscosity tensor results in increased stability [26,27,29–31,34,35]. We have also identified several situations where the interaction between fluid flow and a compliant substrate is of interest [5,6,9,10,37,39]. However, it is still unknown how the odd viscosity will behave when a thin liquid flows over a compliant substrate. Our new model assumes that the fluid's time-reversal symmetry is broken when it flows over a thin compliant substrate. Our objective is to derive the appropriate governing equations, investigate the interdependence of the equations under different conditions, and determine whether the odd viscosity attenuates or intensifies instabilities in the presence of a thin compliant substrate. It is anticipated that the properties of a thin compliant substrate would significantly affect the dynamics of a falling film when the time-reversal symmetry of the liquid is disrupted. The role of odd viscosity will be crucial in determining the stability and dynamics of a thin liquid film on a compliant substrate. Ultimately, we aim to contribute to a better understanding of the underlying instability mechanisms associated with the aforementioned practical problems.

We have structured this paper in the following way. In Sec. II, we present the formulation of the governing equations and associated boundary conditions. Using a long-wave technique, we derive a pair of coupled equations for the film thickness and wall deflection in the presence of odd viscosity in Sec. III. The linear stability analysis is carried out in Sec. IV. We discuss the dynamics of the weakly nonlinear equations as an extension of the Kuramoto-Sivashinsky equation in the presence of odd viscosity in Sec. V. We simulate nonlinear evolution equations in Sec. VI. In Sec. VII, we present a design of the experimental setup. Finally, we discuss our key findings in Sec. VIII.

II. MATHEMATICAL FORMULATION

We investigate the behavior of a two-dimensional, incompressible, viscous, gravity-driven thin liquid film flowing over an inclined (making an angle β with the horizontal), impermeable, infinitely long, and sufficiently thin compliant substrate. The configuration of the flow is depicted in Fig. 1. We adopt a Cartesian coordinate system (x, z), where the x and z axes correspond to the streamwise and cross-stream directions, respectively. The representation of the substrate's shape (solid-liquid interface) and the height of the liquid-air interface at any given moment are given by $z = -s(x, t)$ and $z = h(x, t)$, respectively. Initially, the compliant substrate and thin liquid are positioned at $z = 0$ and $z = H$, respectively, where H represents the thickness of the liquid film in the planar parallel base state. Therefore, we use $z = -s(x, t)$ to indicate the instantaneous displacement of the substrate from its equilibrium position $z = 0$ at time t. Similarly, we use $z = h(x, t)$ to indicate the instantaneous height of the liquid-air interface relative to the equilibrium position $z = 0$. A motionless, inviscid gas surrounds the free surface of the liquid film.

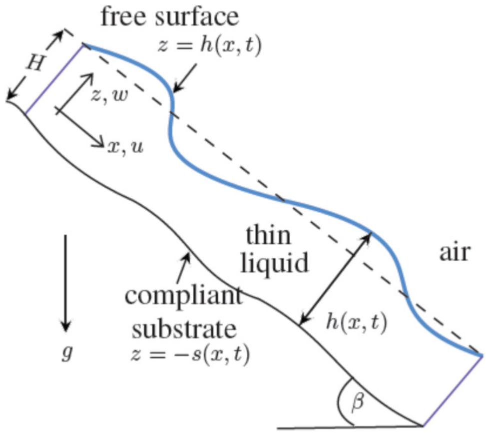

FIG. 1. Schematic of the problem.

If the liquid film is isotropic, then the Cauchy stress tensor τ_{ij} and rate of strain tensor ϑ_{ij} are related linearly as $\tau_{ij} = \mu_{ijkl}\vartheta_{kl}$, where μ_{ijkl} is the viscosity tensor, and $\vartheta_{ij} = (\partial_j\vartheta_i + \partial_i\vartheta_j)/2$, with ϑ_i $(i = 1, 2)$ being the components of the fluid velocity field. The viscosity tensor μ_{ijkl} is symmetric under the exchanges $i \leftrightarrow j$ and $k \leftrightarrow l$ if the total external torque is zero, as dictated by the conservation of angular momentum. Nonetheless, the viscosity tensor can be divided into two parts, even (symmetric) and odd (antisymmetric), under such an exchange as [25] $\mu_{ijkl} = \mu^e_{ijkl} + \mu^o_{ijkl}$, where $\mu^e_{ijkl} = \mu^e_{klij}$ and $\mu^o_{ijkl} = -\mu^o_{klij}$. If the time-reversal symmetry is preserved, then the antisymmetric part drops out. However, in chiral active liquids composed of self-spinning objects subject to torque, the time-reversal symmetry breaks down either naturally or due to an external magnetic field or rotation [17]. For such cases, we must consider the split viscosity tensor as mentioned earlier. Due to this split, the Cauchy stress tensor τ_{ij} consists of two parts [31],

$$\tau_{ij} = \tau^e_{ij} + \tau^o_{ij}, \tag{1}$$

where $\tau^e_{ij} = \mu^e(\partial_i\vartheta_j + \partial_j\vartheta_i)$ is the standard (even) Cauchy stress tensor with standard (even) viscosity coefficient μ^e and $\tau^o_{ij} = \mu^o(\partial_i\vartheta^*_j + \partial^*_i\vartheta_j)$ is the odd part of the Cauchy stress tensor with odd viscosity coefficient μ^o. Here $a^*_i = \epsilon_{ij}a_i$ is the Levi-Civita antisymmetric tensor in two dimensions [23]. In our usual notation, $\tau^o_{xx} = -\mu^o(u_z + w_x)$, $\tau^o_{xz} = \tau^o_{zx} = \mu^o(u_x - w_z)$, and $\tau^o_{zz} = \mu^o(u_z + w_x)$. Here u and w are the components of the velocity vector along x and z directions, respectively. It is to be noted that under the exchange of the indices $x \leftrightarrow z$, the stress tensor due to even viscosity is always symmetric. In contrast, the stress tensor due to odd viscosity contains symmetric $(\tau^o_{xz}, \tau^o_{zx})$ as well as antisymmetric $(-\tau^o_{xx}, \tau^o_{zz})$ parts.

This study considers the physical properties of the liquid, including density ρ, surface tension σ, even viscosity coefficient μ^e, and odd viscosity coefficient μ^o. The primary objective is to investigate the impact of μ^o on the dynamics and stability of liquid film flow over a sufficiently thin compliant substrate.

The governing equations are the conservation of mass and momentum for the flow of the liquid layer $[-s(x,t) \leqslant z \leqslant h(x,t)]$, which are given below

$$u_x + w_z = 0, \tag{2}$$

$$\rho(u_t + uu_x + wu_z) = -p_x + \rho g \sin\beta + \mu^e(u_{xx} + u_{zz}) - \mu^o(w_{xx} + w_{zz}), \tag{3}$$

$$\rho(w_t + uw_x + ww_z) = -p_z - \rho g \cos\beta + \mu^e(w_{xx} + w_{zz}) + \mu^o(u_{xx} + u_{zz}), \tag{4}$$

where g refers to the gravity acceleration.

Given the assumption of the substrate being impermeable, infinitely long, isotropic, and sufficiently thin such that the tension $\mathbb{T}$ remains uniform across its thickness, we can ignore the impact of bending stresses [11,40]. The substrate's motion is also assumed to be slow, so the inertia on the substrate is negligible [14]. Considering that the substrate deflection is only along the normal direction, we have focused on the normal forces along the wall-liquid interface. The balance of the normal forces on the compliant substrate $z = -s(x, t)$ is given by

$$\begin{aligned} p - p_s - \big[2\mu^e\big\{u_x s_x^2 - (u_z + w_x)s_x + w_z\big\} + \mu^o\big\{(u_z + w_x)\big(1 - s_x^2\big) \\ - 2(u_x - w_z)s_x\big\}\big]\big(1 + s_x^2\big)^{-1} + \mathbb{T}s_{xx}\big(1 + s_x^2\big)^{-3/2} = \rho_s h_s d_s s_t\big(1 + s_x^2\big)^{-1/2}, \end{aligned} \tag{5}$$

where ρ_s, h_s, and d_s are the density, thickness, and damping coefficient of the substrate, respectively. A brief derivation of Eq. (5) is provided in the Appendix. Here p_s represents the pressure external to the substrate when the compliant substrate is at its static state ($z = 0$). Consequently,

$$p_s = p_\infty + \rho g H \cos\beta, \tag{6}$$

where p_∞ denotes the atmospheric pressure.

Since the substrate is impermeable, the usual no-slip and kinematic boundary conditions apply on the surface of the substrate $z = -s(x, t)$, which are expressed as follows:

$$u = 0, \tag{7}$$

$$w = -s_t. \tag{8}$$

The conditions governing the behavior of the free interface at $z = h(x, t)$ involve the balance of normal and tangential stresses, as well as the kinematic condition that describes the movement of the surface. These conditions can be expressed as

$$\mu^e\big[(u_z + w_x)\big(1 - h_x^2\big) - 2(u_x - w_z)h_x\big] + \mu^o\big[(u_x - w_z)\big(1 - h_x^2\big) + 2(u_z + w_x)h_x\big] = 0, \tag{9}$$

$$\begin{aligned} p_\infty - p + \big[2\mu^e\big\{u_x h_x^2 - (u_z + w_x)h_x + w_z\big\} + \mu^o\big\{(u_z + w_x)\big(1 - h_x^2\big) - 2(u_x - w_z)h_x\big\}\big] \\ \times \big(1 + h_x^2\big)^{-1} = \sigma h_{xx}\big(1 + h_x^2\big)^{-3/2}, \end{aligned} \tag{10}$$

$$w = h_t + u h_x. \tag{11}$$

III. NONDIMENSIONALIZATION AND MODEL SIMPLIFICATION

We can express the significance of viscous and gravitational forces in the system by using the viscous-gravity length scale, $l_\nu = (\nu^2/g\sin\beta)^{1/3}$, and the viscous-gravity timescale, $t_\nu = [\nu/(g\sin\beta)^2]^{1/3}$ [3,41], where $\nu = \mu^e/\rho$ is the kinematic viscosity. We will use these scales to write the governing equations and boundary conditions in dimensionless form, following the nondimensionalization approach of Chao and Ding [14]. The dimensionless variables, marked by an asterisk in the superscript, are defined as

$$\begin{aligned} &(x, z, h, s) = H(x^*, z^*, h^*, s^*),\ t = (l_\nu t_\nu/H)t^*,\ (u, w) = [H^2/(l_\nu t_\nu)](u^*, w^*), \\ &p = p_\infty + \big(\rho l_\nu H/t_\nu^2\big)p^*. \end{aligned} \tag{12}$$

By utilizing the dimensionless variables outlined in (12), the governing equations (2)–(4), and the boundary conditions (5), (7)–(11) can be expressed in a simplified form, with the asterisk sign removed [31]. The resulting equations are

(i) Governing equations:

$$u_x + w_z = 0, \tag{13}$$

$$3\text{Re}(u_t + uu_x + wu_z) = 1 - p_x + u_{xx} + u_{zz} - \mu(w_{xx} + w_{zz}), \tag{14}$$

$$3\text{Re}(w_t + uw_x + ww_z) = -p_z - \cot\beta + w_{xx} + w_{zz} + \mu(u_{xx} + u_{zz}), \tag{15}$$

where $\mathrm{Re} = gH^3 \sin\beta/(3\nu^2)$ is the Reynolds number and $\mu = \mu^o/\mu^e$ is the odd viscosity coefficient [31].

(ii) Boundary conditions at $z = -s(x,t)$:

$$p = \cot\beta + \left[2\left\{u_x s_x^2 - (u_z + w_x)s_x + w_z\right\} + \mu\left\{(u_z + w_x)\left(1 - s_x^2\right) - 2(u_x - w_z)s_x\right\}\right]\left(1 + s_x^2\right)^{-1} - W_s s_{xx}\left(1 + s_x^2\right)^{-3/2} + B_s s_t\left(1 + s_x^2\right)^{-1/2}, \tag{16}$$

$$u = 0, \tag{17}$$

$$w = -s_t, \tag{18}$$

where $W_s = \mathbb{T}/(\rho g H^2 \sin\beta)$ is a dimensionless tension coefficient and $B_s = \rho_s h_s d_s H/\mu^e$ is a dimensionless damping number which measures the wall damping effects. We have used the relation (6) while deriving Eq. (16).

(iii) Boundary conditions on the free surface $z = h(x,t)$:

$$(u_z + w_x)\left(1 - h_x^2\right) - 2(u_x - w_z)h_x + \mu\left\{(u_x - w_z)\left(1 - h_x^2\right) + 2(u_z + w_x)h_x\right\} = 0, \tag{19}$$

$$p = \left[2\left\{u_x h_x^2 - (u_z + w_x)h_x + w_z\right\} + \mu\left\{(u_z + w_x)\left(1 - h_x^2\right) - 2(u_x - w_z)h_x\right\}\right]\left(1 + h_x^2\right)^{-1} - \mathrm{We}\, h_{xx}\left(1 + h_x^2\right)^{-3/2}, \tag{20}$$

$$w = h_t + u h_x, \tag{21}$$

where $\mathrm{We} = \sigma/(\rho g H^2 \sin\beta)$ is the Weber number.

We can derive a long-wave expansion of the governing equations and their associated boundary conditions by introducing a small parameter ϵ ($\ll 1$) through the transformations $(\partial_t, \partial_x) \to \epsilon(\partial_t, \partial_x)$ and $w \to \epsilon w$ [3]. By applying these transformations in the system of Eqs. (13)–(21) and retaining terms up to $O(\epsilon)$, we arrive at the following equations:

$$u_x + w_z = 0, \tag{22}$$

$$3\epsilon \mathrm{Re}(u_t + u u_x + w u_z) = 1 - \epsilon p_x + u_{zz} - \epsilon \mu w_{zz}, \tag{23}$$

$$p_z + \cot\beta = \epsilon w_{zz} + \mu u_{zz}, \tag{24}$$

$$p = \cot\beta + 2\epsilon(w_z - u_z s_x) + \mu u_z - \epsilon^2 W_s s_{xx} + \epsilon B_s s_t \quad \text{at} \quad z = -s, \tag{25}$$

$$u = 0 \quad \text{at} \quad z = -s, \tag{26}$$

$$w = -s_t \quad \text{at} \quad z = -s, \tag{27}$$

$$u_z + \epsilon\mu\{(u_x - w_z) + 2u_z h_x\} = 0 \quad \text{at} \quad z = h, \tag{28}$$

$$p = 2\epsilon(w_z - u_z h_x) + \mu u_z - \epsilon^2 \mathrm{We}\, h_{xx} \quad \text{at} \quad z = h, \tag{29}$$

$$w = h_t + u h_x \quad \text{at} \quad z = h. \tag{30}$$

In order to obtain the system of equations presented above, we made the assumption that Re, μ, ϵB_s, $\epsilon^2 W_s$, and ϵ^2We are all of order unity. Experimental data suggest that the aspect ratio ϵ is small, with values ranging from 2×10^{-7} to 0.0199 for different setups [31,42,43]. These values confirm that $\epsilon \ll 1$, as previously stated [before Eq. (22)]. Our choice to order the flow parameters allows us to incorporate the effects of inertia, surface tension, odd viscosity, wall tension, and damping in the leading-order flow dynamics. Many previous studies on thin films [11,26,27] have assumed large values of We, which is consistent with our assumption. Alekseenko *et al.* [44] also observed large Weber numbers for the maximum viscous solutions used in their experiments.

We further expand the variables u, w, and p asymptotically in powers of $\epsilon(\ll 1)$ as

$$u = u^{(0)} + \epsilon u^{(1)} + \cdots, \quad w = w^{(0)} + \epsilon w^{(1)} + \cdots, \quad p = p^{(0)} + \epsilon p^{(1)} + \cdots. \tag{31}$$

Substituting (31) into the governing equations (22)–(24) as well as the boundary conditions (25)–(30), the solutions are as follows:

(i) Leading-order solutions:

$$u^{(0)} = h(z+s) - \tfrac{1}{2}(z^2 - s^2), \tag{32}$$

$$w^{(0)} = -s_t - \tfrac{1}{2}(z+s)^2 h_x - (h+s)(z+s)s_x, \tag{33}$$

$$p^{(0)} = (\mu + \cot\beta)(h-z) - \epsilon^2 \mathrm{We} h_{xx}. \tag{34}$$

We wish to emphasize that the leading-order pressure solution [as given in Eq. (34)] includes the effect of odd viscosity, which causes an increase in isotropic pressure.

(ii) First-order solutions:

$$\begin{aligned} u^{(1)} = {}& [\cot\beta h_x - \epsilon^2 \mathrm{We} h_{xxx}]\left[\frac{z^2}{2} - \frac{s^2}{2} - h(s+z)\right] + 3\mathrm{Re}\left\{\left[\frac{(z+s)^4}{24} - \frac{(z+s)(h+s)^3}{6}\right]\right. \\ & \left. \times (h+s)(h+s)_x + \left[\frac{(z+s)^3}{6} - \frac{(z+s)(h+s)^2}{2}\right](h+s)_t\right\} - 2\mu(z+s)(h+s)(h+s)_x, \end{aligned} \tag{35}$$

$$\begin{aligned} p^{(1)} = {}& (h-z)h_x + \mu[\epsilon^2 \mathrm{We} h_{xxx} - \cot\beta h_x](h-z) + \left(\frac{3}{2}\mu\mathrm{Re}\left\{\frac{1}{2}\left[\frac{z^3 - h^3}{3} + s^2(h-z)\right]\right.\right. \\ & \left.\left. - h\left[\frac{z^2 - h^2}{2} - s(h-z)\right]\right\} - 2(1+\mu^2)\right)(h+s)(h+s)_x. \end{aligned} \tag{36}$$

We express the kinematic boundary condition (21) in the mass conservation form as follows:

$$(h+s)_t + \partial_x \int_{-s}^{h} [u^{(0)} + \epsilon u^{(1)}] dz = 0. \tag{37}$$

After substituting the leading and first-order solutions given in (32)–(35) into (37), we can obtain the nonlinear evolution equation that governs the interface of a viscous film over a thin compliant substrate under the influence of odd viscosity as follows:

$$\begin{aligned} & (h+s)_t + (h+s)^2(h+s)_x + \epsilon\big[(h+s)^3\big\{\tfrac{2}{5}\mathrm{Re}(h+s)^3(h+s)_x \\ & - \tfrac{1}{3}(\cot\beta h_x - \epsilon^2 \mathrm{We} h_{xxx}) - \mu(h+s)_x\big\}\big]_x = 0, \end{aligned} \tag{38}$$

where the subscript indicates differentiation with respect to the corresponding variable. To eliminate the time derivative of $(h+s)$ at $O(\epsilon)$ in Eq. (38), we utilize the relation $(h+s)_t = -(h+s)^2(h+s)_x + O(\epsilon)$. We define $\Lambda = h + s$ as the dimensionless thickness of the liquid film to simplify Eq. (38), yielding

$$\Lambda_t + \Lambda^2\Lambda_x + \epsilon\left[\frac{2}{5}\mathrm{Re}\Lambda^6\Lambda_x - (\cot\beta h_x - \epsilon^2 \mathrm{We} h_{xxx})\frac{\Lambda^3}{3} - \mu\Lambda^3\Lambda_x\right]_x = 0. \tag{39}$$

We use Eq. (25) to obtain the evolution equation that describes the dynamics of the thin compliant substrate and obtain

$$\epsilon B_s s_t - \epsilon^2 W_s s_{xx} + \epsilon^2 \mathrm{We} h_{xx} - \cot\beta(\Lambda - 1) - \epsilon\Lambda(2s - h)_x + \frac{\epsilon}{2}\mu \mathrm{Re}\Lambda^4\Lambda_x = 0. \tag{40}$$

We can eliminate ϵ by rescaling Eqs. (39) and (40) using the transformation $(x, t) \to \epsilon(x, t)$. This yields the simplified equation

$$\Lambda_t + \Lambda^2\Lambda_x + \left[\frac{2}{5}\mathrm{Re}\Lambda^6\Lambda_x - (\cot\beta h_x - \mathrm{We} h_{xxx})\frac{\Lambda^3}{3} - \mu\Lambda^3\Lambda_x\right]_x = 0, \tag{41}$$

$$B_s s_t - W_s s_{xx} + \mathrm{We} h_{xx} - \cot\beta(\Lambda - 1) - \Lambda(2s - h)_x + \tfrac{1}{2}\mu \mathrm{Re}\Lambda^4\Lambda_x = 0. \tag{42}$$

The nonlinear evolution equation of the interface (38) yields the Benney-type equation of Joo *et al.* [45] when $\mu = s = 0$. Similarly, setting $\mu = 0$ in Eqs. (41) and (42) gives the equations proposed by Chao and Ding [14] for an isothermal environment. Additionally, for large wall damping and tension ($s \to 0$), the film thickness h satisfies

$$h_t + h^2 h_x + \left[\frac{2}{5}\mathrm{Re} h^6\Lambda_x - (\cot\beta h_x - \mathrm{We} h_{xxx})\frac{h^3}{3} - \mu h^3 h_x\right]_x = 0,$$

which is consistent with prior research [43,46–49].

IV. LINEAR STABILITY ANALYSIS

Equations (41) and (42) have the basic solution $\overline{\Lambda} = 1$ and $\overline{s} = 0$. The steady solution is perturbed with an infinitesimal disturbance $(\widehat{\Lambda}, \widehat{s})$. The solution then can be expressed as [14]

$$(\Lambda, s) = (\overline{\Lambda}, \overline{s}) + (\widehat{\Lambda}, \widehat{s}). \tag{43}$$

Substituting (43) in Eqs. (41) and (42) and then linearization yields the following:

$$\widehat{\Lambda}_t + \widehat{\Lambda}_x + \left[\tfrac{2}{5}\mathrm{Re}\widehat{\Lambda}_x - \tfrac{1}{3}(\cot\beta\widehat{h}_x - \mathrm{We}\widehat{h}_{xxx}) - \mu\widehat{\Lambda}_x\right]_x = 0, \tag{44}$$

$$B_s\widehat{s}_t - W_s\widehat{s}_{xx} + \mathrm{We}\widehat{h}_{xx} - \widehat{\Lambda}\cot\beta - (2\widehat{s} - \widehat{h})_x + \tfrac{1}{2}\mu \mathrm{Re}\widehat{\Lambda}_x = 0. \tag{45}$$

We apply a normal mode expansion to the disturbances $\widehat{\Lambda}$ and $\widehat{s}$ as

$$(\widehat{\Lambda}, \widehat{s}) = (\widetilde{\Lambda}, \widetilde{s})\exp(ikx + \omega t) + \text{c.c.}, \tag{46}$$

where $\widetilde{\Lambda}$ and $\widetilde{s}$ $(\widetilde{\Lambda}, \widetilde{s} \ll 1)$ denote infinitesimal disturbances from the uniform flow and c.c. represents the complex conjugate of the preceding term. Here k is the wave number, $\omega = \omega_r + i\omega_i$ is the complex frequency where ω_r, ω_i are the real and imaginary parts, respectively.

Substituting (46) into Eqs. (44) and (45) yields the following eigenvalue problem:

$$\omega\mathbf{s} = \begin{pmatrix} \mathcal{A}_{11} & \mathcal{A}_{12} \\ \mathcal{A}_{21} & \mathcal{A}_{22} \end{pmatrix}\mathbf{s}, \tag{47}$$

where $\mathbf{s} = (\widetilde{\Lambda}, \widetilde{s})^T$ and

$$\mathcal{A}_{11} = -ik + k^2\left[\frac{2}{5}\mathrm{Re} - \frac{1}{3}(\cot\beta + \mathrm{We}k^2) - \mu\right], \quad \mathcal{A}_{12} = \frac{k^2}{3}(\cot\beta + \mathrm{We}k^2),$$

$$\mathcal{A}_{21} = \frac{\mathrm{We}k^2 + \cot\beta - ik\left(1 + \frac{\mu \mathrm{Re}}{2}\right)}{B_s}, \quad \mathcal{A}_{22} = \frac{-k^2(W_s + \mathrm{We}) + 3ik}{B_s}.$$

The dispersion relation we obtain from (47) is

$$\omega^2 - X\omega + Y = 0, \tag{48}$$

TABLE I. Dimensionless parameters and their values

Dimensionless parameters	Symbols	Values	References
Reynolds number	Re	0–10	[11]
Odd viscosity coefficient	μ	0–2	[27,31]
Tension coefficient	W_s	10^2–10^4	[14]
Damping number	B_s	10–10^3	[14]

where

$$X = \mathcal{B}_1 + i\mathcal{B}_2,\ Y = \mathcal{C}_1 + i\mathcal{C}_2,\ \mathcal{B}_1 = \alpha_1 + \beta_1,\ \mathcal{B}_2 = -k + \frac{3k}{B_s},\ \mathcal{C}_1 = \alpha_1\beta_1 - \alpha_2\beta_2 - \mathcal{A}_{12}\delta_1,$$

$$\mathcal{C}_2 = \alpha_1\beta_2 + \alpha_2\beta_1 - \mathcal{A}_{12}\delta_2,\quad \alpha_1 = k^2\big[\tfrac{2}{5}\mathrm{Re} - \tfrac{1}{3}(\cot\beta + \mathrm{We}k^2) - \mu\big],\quad \alpha_2 = -k,$$

$$\beta_1 = \frac{-k^2(W_s + \mathrm{We})}{B_s},\quad \beta_2 = \frac{3k}{B_s},\quad \delta_1 = \frac{\mathrm{We}k^2 + \cot\beta}{B_s},\quad \delta_2 = \frac{-k\big(1 + \frac{\mu\mathrm{Re}}{2}\big)}{B_s}.$$

Solving (48) and separating the real and imaginary parts gives the expressions of ω_i and ω_r as [50]

$$\omega_i = \frac{\mathcal{B}_2 \pm \sqrt{\frac{\sqrt{\chi_1^2+\chi_2^2}-\chi_1}{2}}}{2},\quad \omega_r = \frac{\mathcal{B}_1 \pm \sqrt{\frac{\sqrt{\chi_1^2+\chi_2^2}+\chi_1}{2}}}{2}, \tag{49}$$

where $\chi_1 = \mathcal{B}_1^2 - \mathcal{B}_2^2 - 4\mathcal{C}_1$ and $\chi_2 = 2\mathcal{B}_1\mathcal{B}_2 - 4\mathcal{C}_2$.

Using $h = \overline{h} + \widetilde{h}\exp(ikx + \omega t) = 1 + \widetilde{h}\exp(ikx + \omega t)$ in the surface evolution equation in the absence of the compliant wall and then linearizing we obtain the dispersion relation as follows:

$$\omega + ik + \left[\frac{k^2}{3}(\cot\beta + k^2\mathrm{We}) + k^2\left(\mu - \frac{2}{5}\mathrm{Re}\right)\right] = 0, \tag{50}$$

where

$$\omega_i = -k,\quad \omega_r = k^2\left[\left(\frac{2}{5}\mathrm{Re} - \mu\right) - \frac{1}{3}(\cot\beta + k^2\mathrm{We})\right]. \tag{51}$$

To discuss the results, we first consider the ranges of different flow parameters according to their order [see after Eq. (30)]. In the investigation by Chao and Ding [14], the stabilizing role of the inclination angle β on the flow of a thin film over a compliant substrate was observed. The influence of the Weber number We is also well established in the literature [3]. As a result, our study does not focus on examining the impact of β and We. Therefore, we set $\beta = \pi/2$ and $\mathrm{We} = 10^2$ [50,51] as fixed parameters for the ensuing discussion. Table I provides the values of the remaining important physical parameters for our study.

The growth rate variation with wave number is depicted in Fig. 2 for different μ values. The parameters We, W_s, and B_s are set to 10^2, 10^2, and 10, respectively. The plot shows a cut-off wave number below which the disturbance amplitude growth rate increases and above which it decreases. As μ increases for a given Re, this phenomenon reduces, indicating the crucial stabilizing role of odd viscosity. Additionally, the figure demonstrates that the real temporal growth rate increases with Re, highlighting that fluid inertia is destabilizing. However, the presence of odd viscosity can significantly suppress this destabilizing behavior induced by inertia.

To analyze the effect of a compliant substrate on the real temporal growth rate, we set $\mathrm{Re} = 5$ and $\mathrm{We} = 10^2$, and plot the results for $(W_s, B_s) = (10^2, 10)$ in Fig. 3(a), obtained from Eqs. (50) and (52). The figure illustrates that the growth rate curves for a compliant substrate ($s \neq 0$) always lie above those for a rigid substrate ($s = 0$), indicating that instability is enhanced when the substrate is compliant, given a value of μ. However, the presence of odd viscosity can suppress the instability

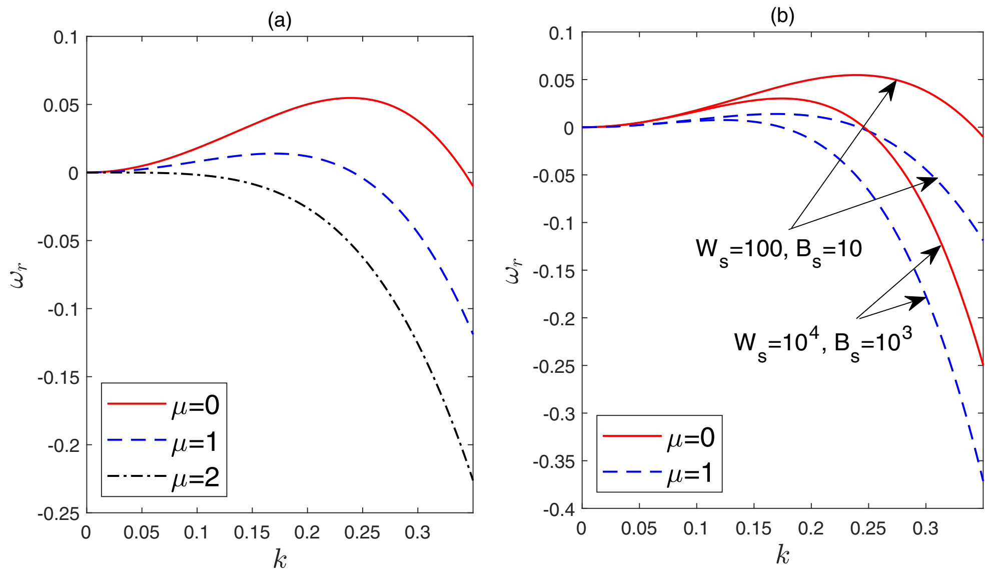

FIG. 2. Influence of μ on the real temporal growth rate as a function of wave number (a) for a very compliant substrate ($W_s = 10^2, B_s = 10$); (b) comparison between a very rigid and very compliant substrate. The other fixed parameters are Re $= 5$ and We $= 10^2$.

for both rigid and compliant substrates. We can investigate this effect further by increasing the wall damping and wall tension coefficients from small values $(W_s, B_s) = (10^2, 10)$ to very large values $(W_s, B_s) = (10^3, 10^2)$ while holding other parameters constant as in Fig. 3(a). Figure 3(b) shows that the compliant substrate can be recovered as a rigid substrate with increasing wall damping and wall tension coefficients.

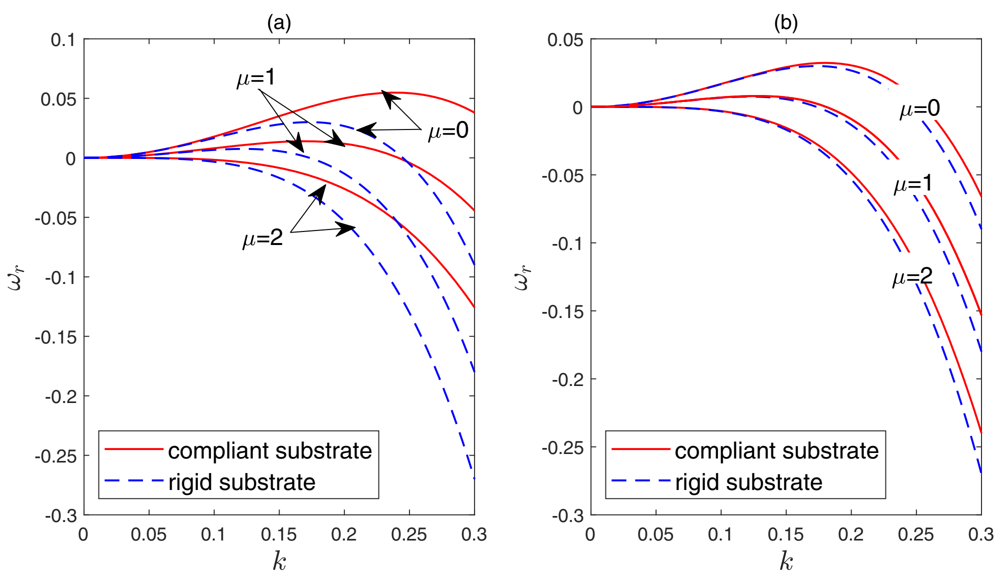

FIG. 3. Growth rate as a function of wave number for (a) $(W_s, B_s) = (10^2, 10)$; (b) $(W_s, B_s) = (10^3, 10^2)$ with fixed Re $= 5$ and We $= 10^2$.

The linear stability analysis presented in the preceding discussion provides valuable insight into the stability mechanism of the two key factors we have investigated: compliant substrate and odd viscosity. Specifically, we can observe that the instability of the thin liquid film flowing over a sufficiently thin compliant substrate is significantly amplified compared to the instability observed when the film flows over a rigid substrate. This is because the damping effect of a rigid substrate is stronger, causing smaller deformations of the liquid-air interface compared to a highly compliant substrate. However, the odd viscosity tensor's presence can suppress this instability. This is due to the fact that the hydrostatic pressure stabilizes the flow by pulling the liquid away from the crest that has been disturbed, and the odd viscosity coefficient μ contributes to this hydrostatic pressure. Therefore, the presence of μ increases the hydrostatic pressure, leading to a more stabilized flow. In summary, the effect of the odd viscosity coefficient μ can counteract the destabilizing influence of a compliant substrate and result in a more stable flow.

V. WEAKLY NONLINEAR EVOLUTION EQUATIONS

Studying a system's weakly nonlinear limit is crucial for understanding its behavior and the impact of nonlinearity on the flow. To achieve this, we make use of a simplified model by introducing substitutions of $h = 1 + \epsilon \breve{h}$ and $s = \epsilon \breve{s}$, which are then substituted into Eq. (39). This leads to the following equation:

$$\breve{\Lambda}_t + \breve{\Lambda}_x + 2\epsilon \breve{\Lambda}\breve{\Lambda}_x + \epsilon\left[\frac{2}{5}\mathrm{Re}\breve{\Lambda}_{xx} + \frac{\epsilon^2}{3}\mathrm{We}\breve{h}_{xxxx} - \mu\breve{\Lambda}_{xx}\right] + O(\epsilon^2) = 0. \tag{52}$$

Applying $\widetilde{x} = x - t, \widetilde{t} = \epsilon t$ [3] and using the chain rule as $(\partial_t)_x = (\partial_{\widetilde{x}})_{\widetilde{t}}(\widetilde{x}_t)_x + (\partial_{\widetilde{t}})_{\widetilde{x}}(\widetilde{t}_t)_x = \epsilon(\partial_{\widetilde{t}})_{\widetilde{x}} - (\partial_{\widetilde{x}})_{\widetilde{t}}$, Eq. (52) yields

$$\breve{\Lambda}_{\widetilde{t}} + 2\breve{\Lambda}\breve{\Lambda}_{\widetilde{x}} + \frac{2}{5}\mathrm{Re}\breve{\Lambda}_{\widetilde{x}\widetilde{x}} + \frac{\epsilon^2}{3}\mathrm{We}\breve{h}_{\widetilde{x}\widetilde{x}\widetilde{x}\widetilde{x}} - \mu\breve{\Lambda}_{\widetilde{x}\widetilde{x}} = 0. \tag{53}$$

It is worth noting that the linear first derivative term $\breve{\Lambda}_x$ can be eliminated through the use of a moving coordinate transformation $\widetilde{x} = x - t$. We further introduce the scalings $\widetilde{t} = \mathcal{G}_1 t^\times, \widetilde{x} = \mathcal{G}_2 x^\times$ and $(\breve{\Lambda}, \breve{h}, \breve{s}) = \mathcal{G}_3(\Lambda^\times, h^\times, s^\times)$ which yields the fluid depth equation in its canonical form after dropping the $^\times$ sign as

$$\Lambda_t + \Lambda\Lambda_x + \Lambda_{xx} + h_{xxxx} = 0, \tag{54}$$

where

$$\mathcal{G}_1 = \frac{25}{3}\frac{\epsilon^2\mathrm{We}}{(2\mathrm{Re} - 5\mu)^2}, \quad \mathcal{G}_2 = \sqrt{\frac{5}{3}\frac{\epsilon^2\mathrm{We}}{(2\mathrm{Re} - 5\mu)}}, \quad \mathcal{G}_3 = \frac{1}{10}\sqrt{\frac{3}{5}\frac{(2\mathrm{Re} - 5\mu)^3}{\epsilon^2\mathrm{We}}}. \tag{55}$$

Repeating the above procedure for Eq. (40), we obtain

$$Ms_x + Ns_{xx} - h_{xx} = 0, \tag{56}$$

where

$$M = \sqrt{\frac{5B_s^2}{3\mathrm{We}(2\mathrm{Re} - 5\mu)}}, \quad N = \frac{W_s}{\mathrm{We}}. \tag{57}$$

Equations (54) and (56) represent a more generalized form of the Kuramoto-Sivashinsky equation for a compliant substrate, incorporating the odd viscosity coefficient μ. The parameter M represents the ratio of wall damping, inertia, and surface tension forces, while N represents the ratio of wall tension and surface tension. An increase in wall damping leads to an increase in the value of M, while an increase in wall tension leads to an increase in the value of N. It is worth noting that the value of M is dependent on μ, whereas N is not affected by the odd viscosity coefficient.

To study the dynamics of the system in the weakly nonlinear regime, we scale Eqs. (54) and (56) as per [11]

$$x \to \frac{L}{\pi}x, \quad t \to \left(\frac{L}{\pi}\right)^2 t, \quad (\Lambda, h, s) \to \frac{\pi}{L}(\Lambda, h, s), \tag{58}$$

and therefore Eqs. (54) and (56) become

$$\Lambda_t + \Lambda\Lambda_x + \Lambda_{xx} + Ph_{xxxx} = 0, \tag{59}$$

$$Qs_x + Ns_{xx} - h_{xx} = 0, \tag{60}$$

where $P = (\pi/L)^2$ and $Q = ML/\pi$.

To obtain periodic solutions of the weakly nonlinear equations, we set the initial conditions as [11]

$$h(x, 0) = 0.02 \cos x, \quad s(x, 0) = 0. \tag{61}$$

To measure the energy transfer from the base flow into the disturbances, we define an energy norm [11,51] in the following form:

$$E_2 = \int_0^L h^2 dx. \tag{62}$$

To begin with, we examine how the flow dynamics for a rigid substrate are impacted by the parameter P, in the absence of odd viscosity. This will be achieved by analyzing the pattern of E_2 curves for various domain sizes L. Next, we investigate the impact of the odd viscosity coefficient μ on the E_2 curves. To focus on weakly nonlinear dynamics, we set the computational domain to $L = 2\pi$. The parameter N, which is related to wall tension, is independent of μ. Matar *et al.* [11] previously established that reducing wall tension results in an increase in chaotic oscillations within a fixed domain. Thus, in this study, we primarily focus on the parameter M, which is influenced by μ.

Matar *et al.* [11] studied the dynamics of falling liquid films on flexible inclines using long-wave theory and the integral method to derive evolution equations for film thickness and substrate deflection at low and moderate Reynolds numbers while maintaining time-reversal symmetry. Similarly, Chao and Ding [14] used the long-wave model developed in Ref. [11] to investigate the behavior of nonisothermal environments. In our study, we extend the existing frameworks for low Reynolds numbers presented in Refs. [11,14] by incorporating the concept of odd viscosity and analyzing the system in the weakly nonlinear limit. Our aim is to gain a deeper understanding of the underlying mechanisms and potentially uncover new insights into the behavior of the system.

Figure 4 depicts the variation of E_2 with respect to the length of the computational domain L, while keeping the support rigid ($Q \to \infty$) and neglecting the odd viscosity μ, as per the study by Matar *et al.* [11]. Three distinct values of P are considered in this analysis, namely 0.45, 0.27, and 0.18. As shown in the figure, the energy norm decreases as P increases (i.e., as L decreases), consistent with the observations of Chao and Ding [14], who noted that short wavelengths tend to damp perturbations. Furthermore, the results of Matar *et al.* [11] suggest that as the domain length increases, the system undergoes bifurcations leading to the formation of different states. These include a "stable single-mode steady state," "single-mode steady traveling waves," and "periodic homoclinic bursts" followed by a "two-mode steady state" [11]. The findings from Fig. 4 align with these observations, confirming similar trends for increasing domain length and emphasizing the crucial role of domain length in flow dynamics. In summary, the outcomes demonstrated in Fig. 4 offer valuable perspectives on the relationship between domain length enlargement and its influence on energy norms and flow dynamics, which could prove helpful in the development and enhancement of fluid systems. Moreover, Fig. 4 highlights that our research aligns with the findings of Matar *et al.* [11] when the fluid retains time-reversal symmetry.

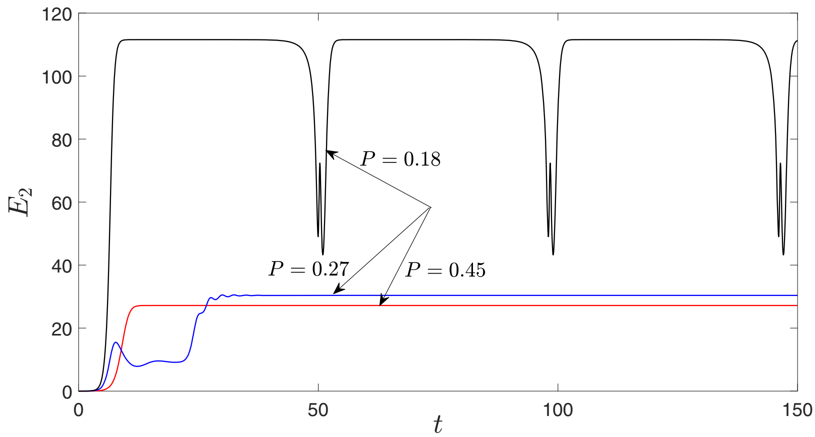

FIG. 4. Evolution of E_2 [from (59) and (60)] for different P in case of a rigid support.

In Fig. 5, we investigate how the compliant substrate affects the temporal evolution of the energy norm E_2 compared to the rigid case in the presence of the odd viscosity coefficient μ. For this analysis, we set $P = 0.18$ as it resulted in "periodic homoclinic bursts" in the rigid substrate case (Fig. 4). The impact of different Q and N values was demonstrated in [11], who studied the case of $P = 0.2$ and observed "periodic homoclinic bursts" with a rigid wall. Among these parameters, we will focus on Q, which is closely linked to our primary parameter of interest, μ. We note that M is a finite positive number when $\mu < (2/5)\text{Re}$, and here we fix $\text{Re} = 5$, so $\mu \in [0, 2)$. We consider the case where $\mu = 0$ [Fig. 5(a)] and for $\mu \neq 0$ [Figs. 5(b)–5(d)], we choose three representative values of $\mu = 0.5, 0.8$, and 1. It is evident from Fig. 5(a) that in the absence of μ, the temporal evolution of the energy norm exhibits significant chaotic oscillations. When we set $\mu = 0.5$ in Fig. 5(b), the chaotic behavior of the E_2 curve completely disappears, although small oscillations are still present. Further increasing μ in Figs. 5(c) and 5(d), we observe that the oscillations are nearly dampened. An increase in μ leads to a rise in M, indicating increased wall damping. Moreover, M and Q have

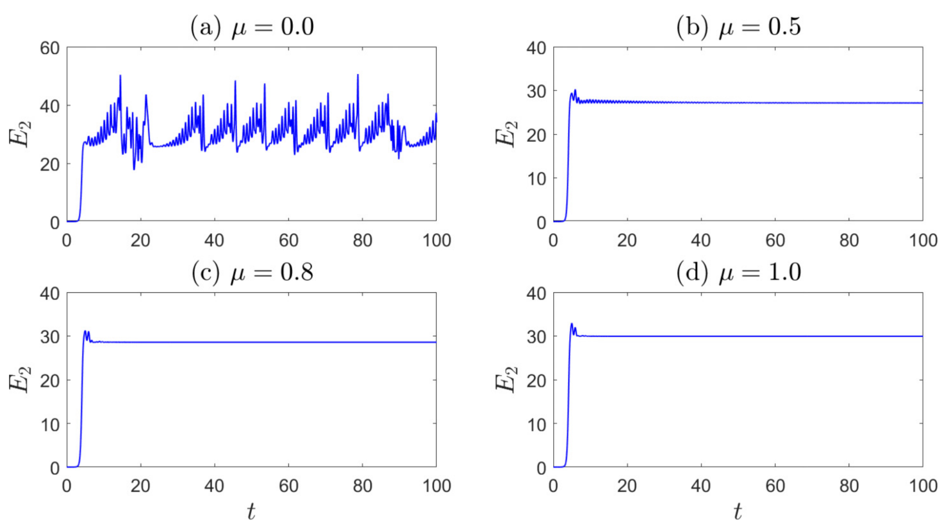

FIG. 5. Evolution of E_2 [from (59) and (60)] for different μ with fixed $P = 0.18$, $\text{Re} = 5$, $\text{We} = 10^2$, $B_s = 10$, and $W_s = 10^2$.

a positive correlation, with an increase in M resulting in a corresponding increase in Q. Matar *et al.* [11] observed that an increase in Q causes a shift from chaotic oscillations to time-periodic attracting solutions. In our current study, we have observed a phenomenon similar to that observed by Matar *et al.* [11]. The results presented in Fig. 5 indicate that as M decreases within the weakly nonlinear regime, chaotic oscillations can arise when the substrate is compliant instead of rigid. Therefore, our significant discovery regarding the addition of the odd viscosity term implies that taking into account the odd viscosity tensor component could be advantageous in preventing chaotic behavior in compliant substrates.

The weakly nonlinear analysis offers valuable perspectives on flow dynamics within the weakly nonlinear limit, characterized by high wall damping and tension. This limit is crucial for investigating instability onset and serves as an accessible model for demonstrating the impact of nonlinearity on the flow. Through an examination of the temporal energy evolution, we explore the influence of the odd viscosity term on the flow. Our findings demonstrate that an increase in odd viscosity results in a decrease in chaotic oscillations within the weakly nonlinear limit. This highlights the potential benefits of considering the odd viscosity tensor component for preventing chaotic behavior in compliant substrates.

VI. NUMERICAL SIMULATIONS

We will examine the nonlinear spatiotemporal dynamics in this section by considering the evolution equations (41) and (42). We will apply periodic boundary conditions in the domain $x \in [0, L]$ and approximate the spatial solutions using the discrete Fourier series as [14]

$$\Lambda(x,t) = \sum_{-N/2+1}^{N/2} \widehat{\Lambda}_n \exp\left(in\frac{2\pi}{L}x\right), \quad s(x,t) = \sum_{-N/2+1}^{N/2} \widehat{s}_n \exp\left(in\frac{2\pi}{L}x\right), \tag{63}$$

where the "hat" decorated variables are the Fourier amplitudes of the disturbances and N is the number of Fourier modes. Chattopadhyay *et al.* [30] previously demonstrated the space-time convergence of the numerical scheme used in this study. To further verify the accuracy of our scheme, we conducted a space-time convergence analysis and found that 256 Fourier modes with a time step of 0.01 and an absolute error tolerance of 10^{-6} were sufficient. Additionally, we reproduced the results of Refs. [11,50,52] to ensure the validity of our scheme. While Chao and Ding [14] investigated the impact of computational domain length in their study, we did not explore this factor here. For all our simulations, we set $L = 20\pi$.

Our numerical investigation begins with applying a harmonic perturbation to the liquid film at time $t = 0$, while keeping the compliant substrate flat. The initial condition is chosen as [11]

$$\Lambda(x,0) = 1 + 0.01\exp[-5(x-5)^2], \quad s(x,0) = 0. \tag{64}$$

Figure 6 illustrates the influence of the odd viscosity coefficient μ on the maximum ($h_{\max}$) and minimum ($h_{\min}$) amplitude of the film thickness in the presence of a very compliant substrate over a relatively long time. To plot Fig. 6(a), we choose $\mathrm{Re} = 2$, $\mathrm{We} = 10^2$, $W_s = 10^2$, and $B_s = 10$. We observe from the figure that the disturbance amplitude reduces with the presence of μ. In Fig. 6(b), we investigate the influence of inertia on the film flow by considering $\mathrm{Re} = 10$ and keeping the other parameters the same as Fig. 6(a). We find that the wave amplitude significantly increases with an increase in Re, but μ plays a crucial stabilizing role despite strong inertial effects for $\mu = 0.1$ and $\mu = 0.5$. Figure 6 concludes that the odd viscosity coefficient plays a vital role in stabilizing the liquid flow on a compliant substrate.

Figure 7 illustrates the evolution of the liquid film profile h over time for a highly compliant substrate. To investigate the impact of the odd viscosity coefficient μ at different time intervals ($t = 600$, 800, and 1000), we present Figs. 7(a) (for $\mu = 0$) and 7(b) (for $\mu \neq 0$), respectively. A comparison of these two figures reveals that an increase in μ leads to a decrease in the growth of interfacial waves. We further plot the profile of the liquid film h at $t = 600$ in Fig. 7(c) to

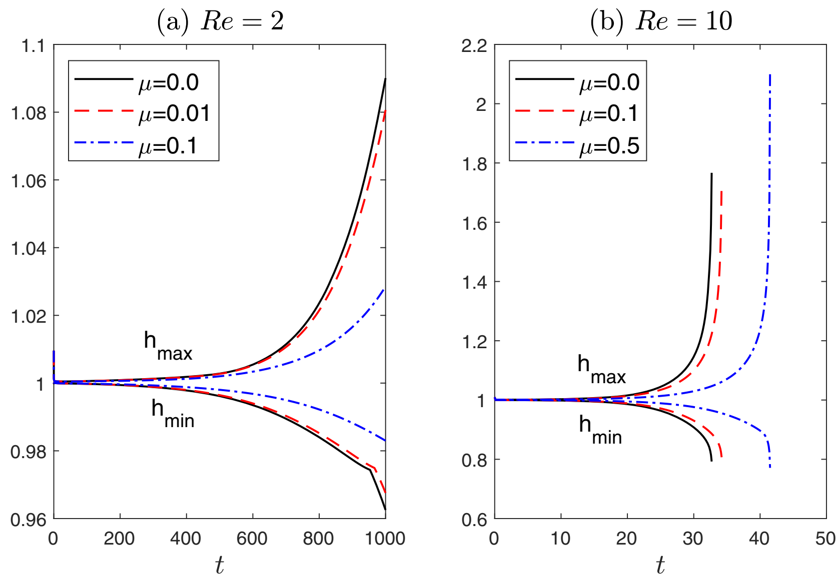

FIG. 6. Maximum ($h_{\max}$) and minimum ($h_{\min}$) amplitude of surface wave instabilities for a thin film flow along a very compliant substrate for different μ with fixed $W_s = 10^2$, $B_s = 10$, and We $= 10^2$.

visualize this reduction more explicitly. The results demonstrate that the crest of the interfacial wave diminishes with increasing μ. Hence, taking into account the odd viscosity effect can reduce instability in the case of a highly compliant substrate.

Figure 8 illustrates the maximum ($s_{\max}$) and minimum ($s_{\min}$) amplitudes of the compliant substrate s for varying values of the odd viscosity coefficient μ over a relatively long time period.

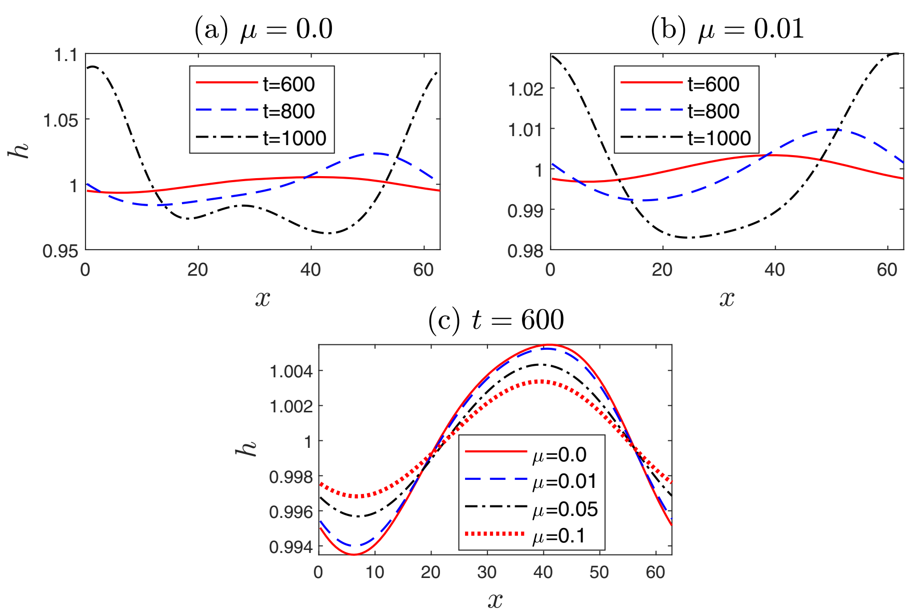

FIG. 7. The profile of liquid film h for a thin film flow along a very compliant substrate with fixed $W_s = 10^2$, $B_s = 10$, Re $= 2$, and We $= 10^2$.

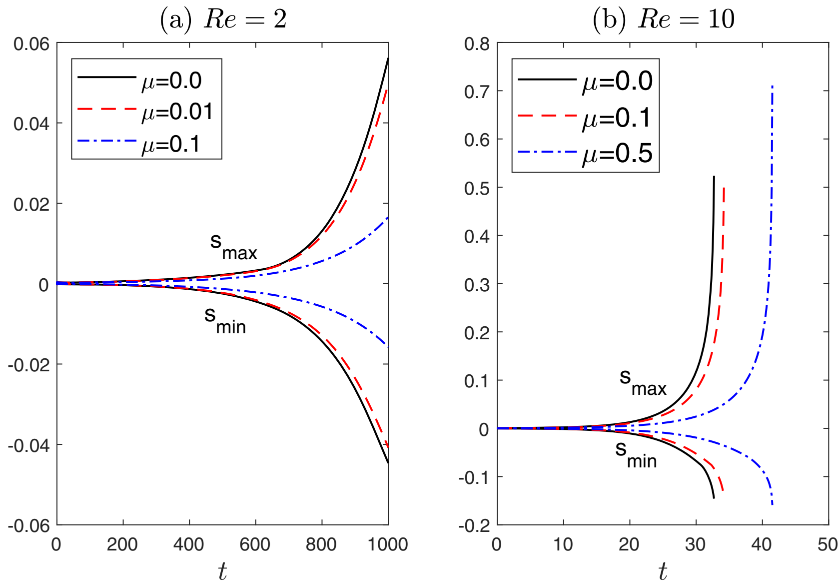

FIG. 8. Maximum (s_{max}) and minimum (s_{min}) amplitude of the substrate s for a thin film flow along a very compliant substrate for different μ with fixed $W_s = 10^2$, $B_s = 10$, and We $= 10^2$.

Our results indicate that for a fixed time t, the growth of the (s_{max}) [and similarly (s_{min})] curves decreases with increasing μ. To investigate the effect of inertia on the substrate, we plot Fig. 8(b). A comparison of Figs. 8(a) and 8(b) clearly shows that although Re enhances the growth of the substrate, μ can effectively stabilize it. We further present the spatial evolution profile of the substrate s in Fig. 9. Here, Figs. 9(a) and 9(b) demonstrate the evolution of s at time $t = 600$, 800, and 1000 in the absence and presence of μ, respectively. A comparison of Figs. 9(a) and 9(b) reveals that the presence of μ significantly affects the evolution of the compliant substrate. In Fig. 9(c), we present the effect of μ at a specific time instant $t = 600$ and observe that the presence of μ stabilizes the deformation of the compliant substrate.

In Fig. 10, we investigate the interplay between the inertia and odd viscosity coefficient μ on the profile of the liquid film h and substrate s for a very compliant substrate at $t = 600$. Figures 10(a) and 10(b) depict the profiles in the absence of μ, revealing that the crest of the wave and substrate height increases with increasing Reynolds number Re. To examine the impact of μ on the profiles of h and s, we use $\mu = 0.1$ in Figs. 10(c) and 10(d). Comparing all the figures shows that the presence of μ plays a crucial role in suppressing the instability.

Figure 11 presents the maximum amplitude of the liquid profile h and substrate s for a highly compliant and a highly rigid substrate, with and without the odd viscosity coefficient μ. To recover a rigid substrate by increasing wall damping and tension, we investigate three sets of parameters: $(W_s, B_s) = (10^2, 10)$, $(W_s, B_s) = (10^3, 10^2)$, and $(W_s, B_s) = (10^4, 10^3)$. Figure 11(a) shows that a rigid substrate promotes flow stability, and the difference in growth of h_{max} is more pronounced as (W_s, B_s) increases from $(10^2, 10)$ to $(10^3, 10^2)$ than from $(10^3, 10^2)$ to $(10^4, 10^3)$. Similar behavior is observed for the s_{max} curves [Fig. 11(b)]. Figures 11(c) and 11(d) demonstrate the stabilizing effect of μ on the h_{max} and s_{max} profiles for both highly compliant and rigid substrates.

Figure 12 shows a snapshot of the liquid film thickness h at $t = 700$ for a highly compliant and rigid substrate with and without the odd viscosity coefficient μ. We use $(W_s, B_s) = (10^2, 10)$ for the highly compliant substrate and $(W_s, B_s) = (10^4, 10^3)$ for the highly rigid substrate. In the absence of the odd part of the viscosity tensor ($\mu = 0$), we observe an enhancement of the crest of waves for the highly compliant substrate, consistent with the findings of Chao and Ding [14].

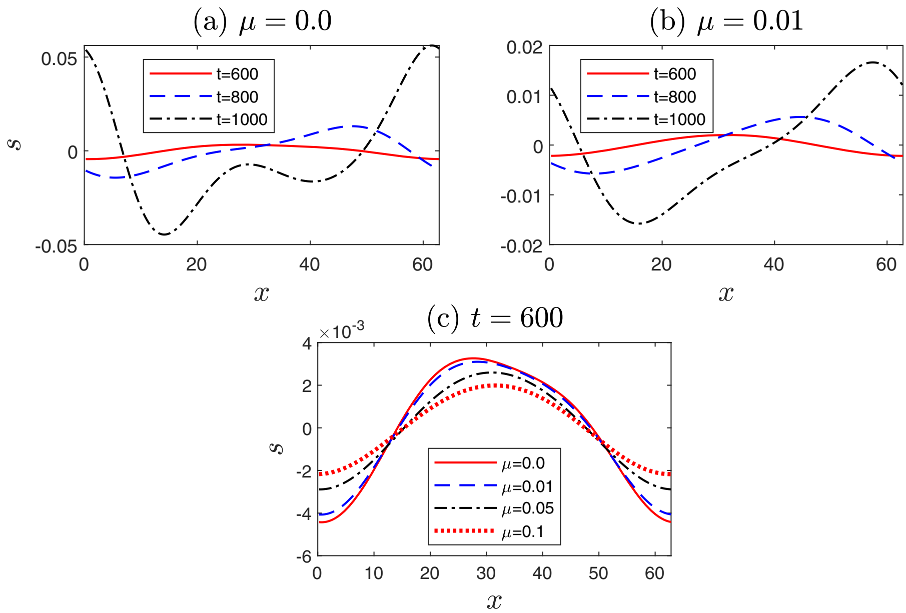

FIG. 9. The profile of substrate s for a thin film flow along a very compliant substrate with fixed $W_s = 10^2$, $B_s = 10$, Re $= 2$, and We $= 10^2$.

However, when we consider the effect of μ ($\mu = 0.05$), the crest of waves reduces with increasing μ for both substrates. Figure 13 shows a similar snapshot for the substrate s, and we observe a similar behavior of the highly compliant substrate and μ as seen in Fig. 12. These results suggest

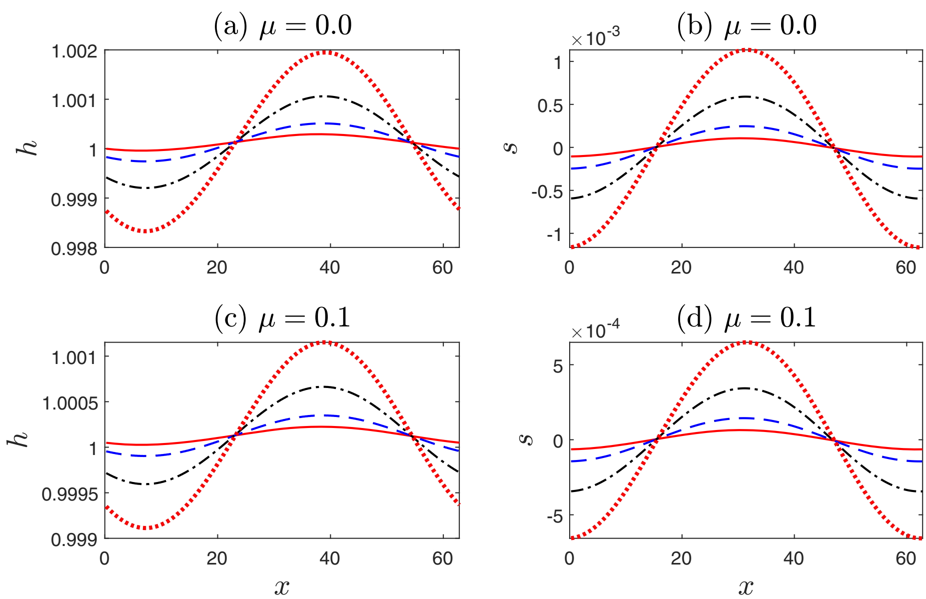

FIG. 10. The profiles of liquid film h and substrate s for a very compliant substrate at $t = 600$ for different Re with fixed $W_s = 10^2$, $B_s = 10$, and We $= 10^2$. Here red solid line (——), blue dashed line (– –), black dot-dashed line (– · –) and red dotted line (· · ·) represent the curves at Re $= 0.4$, 0.8, 1.2, and 1.5, respectively.

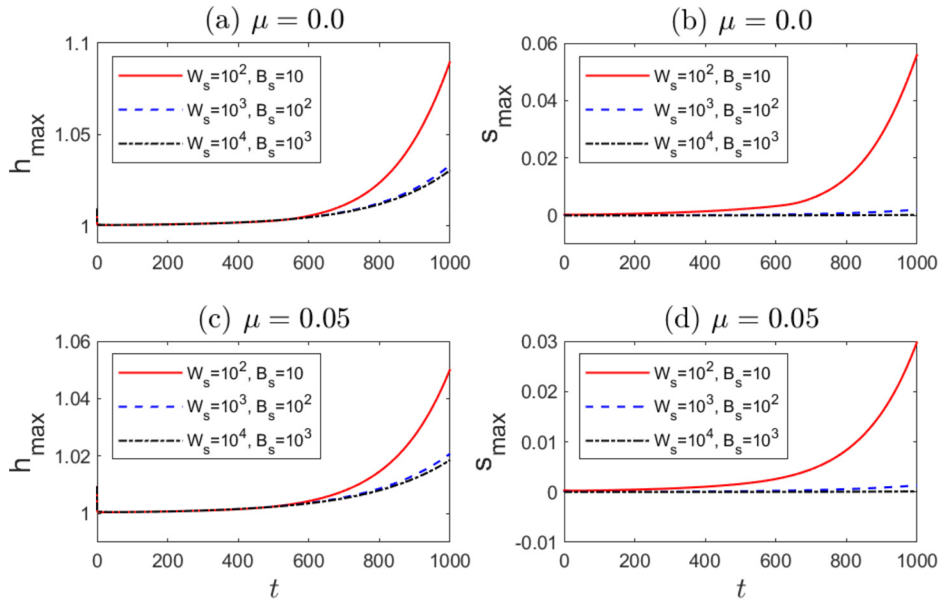

FIG. 11. Maximum amplitude of the liquid film profile h and substrate s for a thin film flow along a very compliant and very rigid substrate for different μ with fixed Re $= 2$ and We $= 10^2$.

that a rigid substrate is always more stable than a compliant one due to the higher values of wall damping and wall tension, which give the rigid substrate a stronger ability to dissipate energy and thus promote flow stability.

The time evolution of the energy norm $E_2 = \int_0^L \Lambda^2 dx$ [51] for a large timescale ($t = 2 \times 10^4$) is presented in Fig. 14 for a very compliant substrate with $(W_s, B_s) = (10^2, 10)$ and a very rigid substrate with $(W_s, B_s) = (10^4, 10^3)$. Initially, the value of the energy norm is nearly parallel to the base flow. As time progresses, the value of E_2 gradually increases until it reaches a certain time $t = t_c$, after which the system evolves into a saturated steady state with a constant energy norm. The

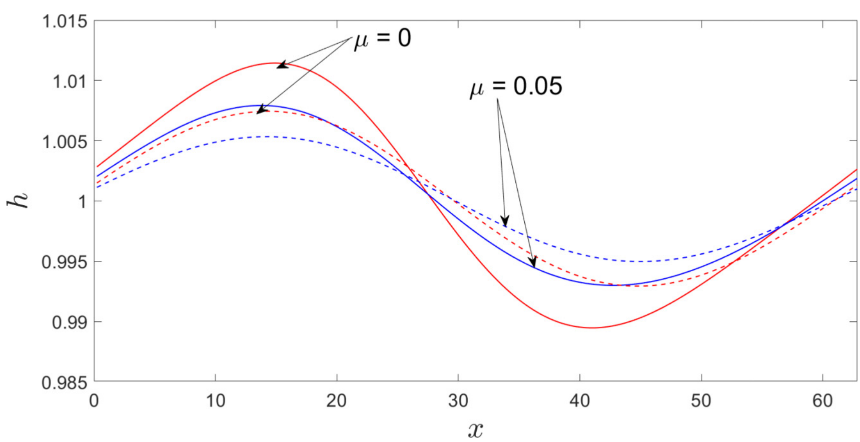

FIG. 12. Spatial evolution of the film thickness h for $(W_s, B_s) = (10^2, 10)$ (very compliant substrate) and $(W_s, B_s) = (10^4, 10^3)$ (very rigid substrate) at $t = 700$ with Re $= 2$ and We $= 10^2$. Here solid line (——) and dashed line (−−) indicate very compliant and very rigid substrate, respectively.

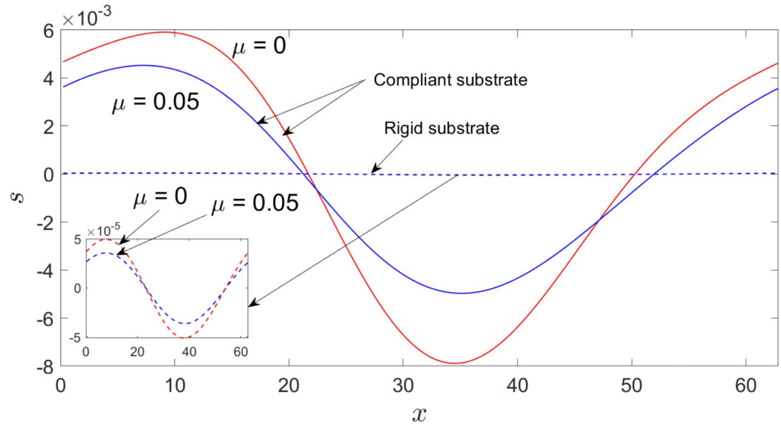

FIG. 13. Spatial evolution of the substrate s for $(W_s, B_s) = (10^2, 10)$ (very compliant substrate) and $(W_s, B_s) = (10^4, 10^3)$ (very rigid substrate) at $t = 700$ with Re = 2 and We = 10^2.

figure shows that the growth rate of the energy norm is higher for a compliant substrate than a rigid one. However, as the odd viscosity coefficient μ increases, the growth rate of E_2 decreases. These time-dependent simulations agree with the findings of the linear stability analysis.

To gain a more comprehensive understanding of the impact that a compliant substrate and odd viscosity have on the stability of thin film flow beyond the point of linear stability, we conducted numerical simulations of the evolution equations in a periodic domain over an extended period of time. The outcome of these simulations demonstrates that a compliant substrate leads to a destabilizing effect, while odd viscosity has a stabilizing influence over time. This analysis provides insights beyond those obtained from the linear stability analysis, resulting in a more nuanced understanding of the system's behavior.

VII. PROPOSED DESIGN OF EXPERIMENTAL SETUP

This section presents an experimental setup for the current study, as illustrated by the two-dimensional (2D) model in Fig. 15. To begin with, a compliant or flexible substrate is required

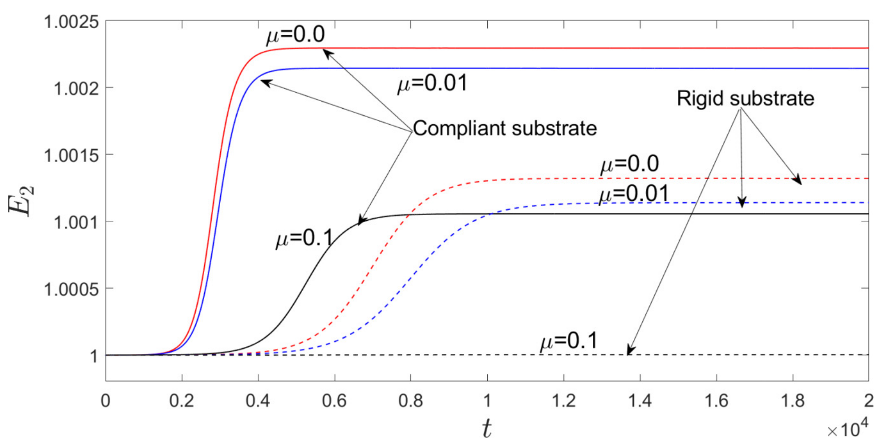

FIG. 14. Temporal evolution of the energy norm E_2 for $(W_s, B_s) = (10^2, 10)$ (very compliant substrate) and $(W_s, B_s) = (10^4, 10^3)$ (very rigid substrate) with Re = 1 and We = 10^2.

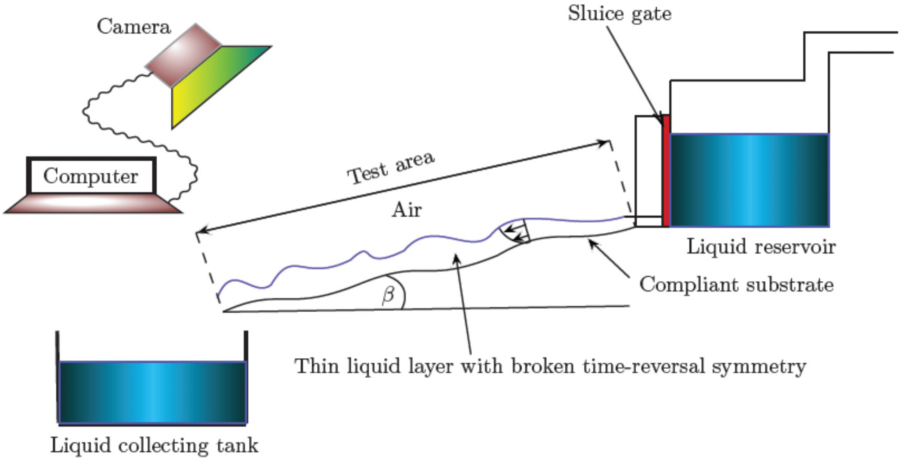

FIG. 15. Two-dimensional model of the experimental setup.

on which a time-reversal symmetry-breaking liquid can flow. The substrate can be made of heat-resistant polymers such as PET or natural rubber. A mechanism to change the inclination angle of the test area is also necessary, as even tiny changes can affect the wave patterns of the thin liquid film. A traversing mechanism can be used for this purpose. It is also essential to have a rigid support to hold the test area in place. To continuously supply the testing area of the compliant substrate with the liquid (with broken time-reversal symmetry), a reservoir needs to be set up. Additionally, a device should be installed to vary the liquid flow rate from the reservoir. A movable gate can be used to adjust the height of the thin liquid. A Sluice gate is the specific device required for an open channel flow. Moreover, the compliant substrate should be wide enough to prevent any liquid from falling off the edge during the formation of the liquid film, which could affect the flow dynamics. Finally, to measure the instability of the flow system, a high-quality digital camera connected to a computer is needed to capture various snapshots. Since the thin liquid flows over a compliant substrate, there is no need for additional devices, such as a speaker, to generate sound waves to examine the stability of the thin film flow in this study.

Our primary goal is to investigate the stabilizing role of odd viscosity to suppress the flow instability due to the compliant substrate to some extent. As an initial step, we will flow a thin liquid (which holds the time-reversal symmetry, i.e., $\mu = 0$) over a rigid and compliant substrate. One has to capture several snapshots at different time instants. This will determine the flow instability enhancement due to the compliant substrate. The next step is to examine the stabilizing role of μ. For that, one has to repeat the earlier procedure for $\mu \neq 0$. To visualize the suppression of flow instability due to μ, one has to capture several snapshots at earlier time instants. In addition, one can examine the growth and reduction of the instability due to compliant substrate and odd viscosity, respectively, by capturing a video of the fluid flow for a specific time.

VIII. SUMMARY AND CONCLUSIONS

This study examines the behavior of a falling viscous liquid over a compliant substrate with broken time-reversal symmetry, incorporating the nondissipative effect of the odd viscosity coefficient. Using the long-wave expansion method, we obtain a set of equations that describe the spatiotemporal evolution of the film thickness and wall deflection, considering the odd viscosity effect. Linear stability analysis shows that the compliant substrate enhances the instability while increasing the odd viscosity coefficient reduces it. The damping effect is weaker for a compliant substrate, making the flow system more unstable, but odd viscosity enhances the stabilizing role of hydrostatic pressure, leading to stabilization. In the weakly nonlinear limit, we derive the evolution equations for the film thickness and wall deflection, which exhibit various effects, such as developing chaotic solutions, for decreasing substrate tension. However, increasing odd viscosity reduces the development of chaotic solutions in this regime. Finally, we perform numerical simulations of the evolution equations in a periodic domain, comparing the results for a very compliant and a very rigid substrate. The simulations demonstrate the stabilizing effect of odd viscosity and destabilizing effect of the compliant substrate at large times, providing a better understanding of odd viscosity's influence beyond the linear stability threshold. When a rigid substrate is present, the damping effect is strong, and the deformations of the liquid-air interface are limited. As a result, a very rigid substrate makes the system more stable, which is confirmed by the temporal evolution of the energy norm. Conversely, a very compliant substrate has weaker damping, leading to larger interface deformations and a more unstable system. However, odd viscosity can counteract the instability caused by a compliant substrate by increasing the hydrostatic pressure.

The studies conducted by Matar *et al.* [11] and Chao and Ding [14] suggest that flexible walls have a destabilizing effect. Carpenter and Garrad [53,54] have also shown that viscoelastic damping can destabilize the Tollmien-Schlichting instability for flexible Kramer-type substrates. However, Brown [55] demonstrated the potential benefits of using compliant substrates in technological applications. Our study concludes that while compliant substrates can enhance surface wave instability, accounting for odd viscosity can alleviate this issue. Furthermore, although fluid inertia amplifies destabilizing behavior, odd viscosity can suppress wave amplitude. These findings have practical implications, particularly in improving product outcomes that involve compliant substrates exacerbating interfacial instabilities. We acknowledge that our current model is a simple one, and we are interested in exploring other models for compliant substrates to investigate interfacial instabilities. In the future, we aim to experimentally verify our study's results and extend our theoretical model to moderate Reynolds numbers.

ACKNOWLEDGMENTS

We express our gratitude to the chief editor and the anonymous referees for their valuable suggestions and insightful comments that have greatly enhanced the quality of this manuscript. A.K.G. acknowledges the Science and Engineering Research Board (SERB) for partially supporting this work through Grant No. S.R.G./2021/001412.

S.C. was responsible for conceptualizing the study, analyzing the results, writing the initial draft, and reviewing and editing the manuscript. A.S.D. and A.K.G. were responsible for software development. A.M. reviewed the work. All authors provided input and feedback on the manuscript and approved the final version. The authors report no conflict of interest.

APPENDIX

Here we present the origin of Eq. (5).

According to Newton's second law, one can express the explicit elasticity equation for the compliant substrate as [15]

$$\rho_s b\mathcal{X}_{tt} + \mathcal{D}(e_z \cdot \mathcal{X}_t)e_z - \left[\frac{\mathbb{T}_x t_s}{\left(1+s_x^2\right)^{1/2}} - \frac{\mathbb{T}\, s_{xx} n_s}{\left(1+s_x^2\right)^{3/2}}\right] + \mathcal{B}(\kappa_s n_s)_{SS} = \tau \cdot n_s + p_s n_s, \tag{A1}$$

where, $\mathcal{X}(S,t) = (X(S,t), Z(S,t))$ is the parametric representation of the substrate, S is the arc length, $(X(S,t), Z(S,t)) = (x, -s(x,t))$ is the reparametrized position of the inclined plane, b is the thickness of the compliant substrate, $\mathcal{D} = \rho_s h_s d_s$, e_z is the unit vector in the z direction, $n_s = (s_x, 1)(1+s_x^2)^{-1/2}$ is the unit normal vector, $t_s = (1, -s_x)(1+s_x^2)^{-1/2}$ is the unit tangent vector, $\mathcal{B}$ is the flexural rigidity, κ_s is the curvature and τ is the liquid stress tensor [see Eq. (1)].

If we assume a small deflection of the thin compliant substrate, then $\rho_s b = \mathcal{B} = 0$ and consequently Eq. (A1) reduces to the following form:

$$\mathcal{D}(e_z \cdot \mathcal{X}_t)e_z - \left[\frac{\mathbb{T}_x t_s}{\left(1+s_x^2\right)^{1/2}} - \frac{\mathbb{T} s_{xx} n_s}{\left(1+s_x^2\right)^{3/2}} \right] = \tau \cdot n_s + p_s n_s. \tag{A2}$$

In the present study, we have considered that the compliant substrate to be sufficiently thin. Therefore, we can assume the wall tension $\mathbb{T}$ to be constant (hence $\mathbb{T}_x = 0$), and hence we neglect the bending stresses [2,11]. Due to the consideration of the small deflection (longitudinal deflections are small compared to transverse deflections) of the substrate, we have to consider the normal component of Eq. (A2) [15], which is given below

$$\mathcal{D}(e_z \cdot \mathcal{X}_t)(e_z \cdot n_s) + \frac{\mathbb{T} s_{xx}}{\left(1+s_x^2\right)^{3/2}} = n_s \cdot \tau \cdot n_s + p_s. \tag{A3}$$

For negligible longitudinal extension (i.e., $X_t \ll Z_t$), $\mathcal{X}_t = (0, -s_t)$. Also, $e_z \cdot \mathcal{X}_t = -s_t$ and $e_z \cdot n_s = (1 + s_x^2)^{-1/2}$. Therefore the boundary condition equation at $z = -s(x, t)$ can be expressed as given in (5). For a more detailed derivation, we refer to the work of Alexander *et al.* [15].

---

[1] A. Oron, S. H. Davis, and S. G. Bankoff, Long-scale evolution of thin liquid films, Rev. Mod. Phys. **69**, 931 (1997).

[2] R. Craster and O. K. Matar, Dynamics and stability of thin liquid films, Rev. Mod. Phys. **81**, 1131 (2009).

[3] S. Kalliadasis, C. Ruyer-Quil, B. Scheid, and M. G. Velarde, Falling liquid films, in *Applied Mathematical Sciences*, Vol. 176 (Springer, Berlin, 2012).

[4] S. Chattopadhyay, A. Mukhopadhyay, and A. K. Barua, A review on hydrodynamical stability of thin film flowing along an inclined plane, J. Math. Sci. Modell. **2**, 133 (2019).

[5] J. Huang, M. Juszkiewicz, W. H. De Jeu, E. Cerda, T. Emrick, N. Menon, and T. P. Russell, Capillary wrinkling of floating thin polymer films, Science **317**, 650 (2007).

[6] T. T. Al-Housseiny, I. C. Christov, and H. A. Stone, Two-Phase Fluid Displacement and Interfacial Instabilities Under Elastic Membranes, Phys. Rev. Lett. **111**, 034502 (2013).

[7] D. Kumar, J. D. Paulsen, T. P. Russell, and N. Menon, Wrapping with a splash: High-speed encapsulation with ultrathin sheets, Science **359**, 775 (2018).

[8] S. Nikravesh, D. Ryu, and Y. Shen, Instabilities of thin films on a compliant substrate: Direct numerical simulations from surface wrinkling to global buckling, Sci. Rep. **10**, 5728 (2020).

[9] D. Halpern and J. B. Grotberg, Fluid-elastic instabilities of liquid-lined flexible tubes, J. Fluid Mech. **244**, 615 (1992).

[10] D. Halpern and J. B. Grotberg, Surfactant effects on fluid-elastic instabilities of liquid-lined flexible tubes: A model of airway closure, J. Biomech. Eng. **115**, 271 (1993).

[11] O. K. Matar, R. V. Craster, and S. Kumar, Falling films on flexible inclines, Phys. Rev. E **76**, 056301 (2007).

[12] G. M. Sisoev, O. K. Matar, R. V. Craster, and S. Kumar, Coherent wave structures on falling fluid films flowing down a flexible wall, Chem. Eng. Sci. **65**, 950 (2010).

[13] P. D. Howell, J. Robinson, and H. A. Stone, Gravity-driven thin-film flow on a flexible substrate, J. Fluid Mech. **732**, 190 (2013).

[14] Y. Chao and Z. Ding, Thermocapillary thin-film flows on a compliant substrate, Phys. Rev. E **99**, 043101 (2019).

[15] J. P. Alexander, T. L. Kirk, and D. T. Papageorgiou, Stability of falling liquid films on flexible substrates, J. Fluid Mech. **900**, A40 (2020).

[16] A. Samanta, Effect of surfactant on the linear stability of a shear-imposed fluid flowing down a compliant substrate, J. Fluid Mech. **920**, A23 (2021).

[17] J. E. Avron, Odd viscosity, J. Stat. Phys. **92**, 543 (1998).
[18] V. Soni, E. S. Bililign, S. Magkiriadou, S. Sacanna, D. Bartolo, M. J. Shelley, and W. T. M. Irvine, The odd free surface flows of a colloidal chiral fluid, Nat. Phys. **15**, 1188 (2019).
[19] A. I. Berdyugin, S. G. Xu, F. M. D. Pellegrino, R. K. Kumar, A. P. Torre, X. B. Shalom, T. T. Watanabe, I. V. Grigorieva, M. P. K. Geim, and D. A. Bandurin, Measuring Hall viscosity of graphene's electron fluid, Science **364**, 162 (2019).
[20] L. Yamauchi, T. Hayata, M. Uwamichi, T. Ozawa, and K. Kawaguchi, Chirality-driven edge flow and non-Hermitian topology in active nematic cells, arXiv:2008.10852.
[21] M. Fruchart, C. Scheibner, and V. Vitelli, Odd viscosity and odd elasticity, Annu. Rev. Condens. Matter Phys. **14**, 471 (2023).
[22] D. Banerjee, A. Souslov, A. Abanov, and V. Vitelli, Odd viscosity in chiral active fluids, Nat. Commun. **8**, 1573 (2017).
[23] S. Ganeshan and A. Abanov, Odd viscosity in two-dimensional incompressible fluids, Phys. Rev. Fluids **2**, 094101 (2017).
[24] A. G. Abanov, T. Can, and S. Ganeshan, Odd surface waves in two-dimensional incompressible fluids, SciPost Phys. **5**, 010 (2018).
[25] M. F. Lapa and T. L. Hughes, Swimming at low Reynolds number in fluids with odd, or Hall, viscosity, Phys. Rev. E **89**, 043019 (2014).
[26] G. Bao and Y. Jian, Odd-viscosity-induced instability of a falling thin film with an external electric field, Phys. Rev. E **103**, 013104 (2021).
[27] S. Chattopadhyay, Thermocapillary instability in the presence of uniform normal electric field: Effect of odd viscosity, J. Eng. Math. **131**, 9 (2021).
[28] J. Zhao and Y. Jian, Effect of odd viscosity on the stability of a falling thin film in presence of electromagnetic field, Fluid Dynam. Res. **53**, 015510 (2021).
[29] B. Jia and Y. Jian, The effect of odd-viscosity on Rayleigh–Taylor instability of a liquid film under a heated inclined substrate, Phys. Fluids **34**, 044104 (2022).
[30] S. Chattopadhyay, G. Y. Subedar, A. K. Gaonkar, A. K. Barua, and A. Mukhopadhyay, Effect of odd-viscosity on the dynamics and stability of a thin liquid film flowing down on a vertical moving plate, Int. J. Non-Lin. Mech. **140**, 103905 (2022).
[31] E. Kirkinis and A. V. Andreev, Odd-viscosity-induced stabilization of viscous thin liquid films, J. Fluid Mech. **878**, 169 (2019).
[32] G. M. Monteiro and S. Ganeshan, Nonlinear shallow water dynamics with odd viscosity, Phys. Rev. Fluids **6**, L092401 (2021).
[33] A. Doak, G. Baardink, P. A. Milewski, and A. Souslov, Nonlinear shallow-water waves with vertical odd viscosity, SIAM J. Appl. Math. **83**, 938 (2023).
[34] S. Chattopadhyay, Odd-viscosity-induced instability of a thin film with variable density, Phys. Fluids **33**, 082102 (2021).
[35] A. Samanta, Role of odd viscosity in falling viscous fluid, J. Fluid Mech. **938**, A9 (2022).
[36] A. S. Desai, S. Chattopadhyay, A. K. Gaonkar, and A. Mukhopadhyay, Shear imposed falling film with odd viscosity effects, Int. J. Non-Lin. Mech. **153**, 104422 (2023).
[37] D. Halpern, H. Fujioka, S. Takayama, and J. B. Grotberg, Liquid and surfactant delivery into pulmonary airways, Respir. Physiol. Neurobiol. **163**, 222 (2008).
[38] J. Whitlock, Blood flow through the heart and lungs, https://www.verywellhealth.com/blood-flow-through-the-heart-3156938.
[39] V. Kumaran, and R. Muralikrishnan, Spontaneous Growth of Fluctuations in the Viscous Flow of a Fluid Past a Soft Interface, Phys. Rev. Lett. **84**, 3310 (2000).
[40] H. B. Atabek and H. S. Lew, Wave propagation through a viscous incompressible fluid contained in an initially stressed elastic tube, Biophys. J. **6**, 481 (1966).
[41] A. Mukhopadhyay, S. Chattopadhyay, and A. K. Barua, Effects of strong viscosity with variable fluid properties on falling film instability, in *Advances in Nonlinear Dynamics*, edited by W. Lacarbonara, B. Balachandran, M. J. Leamy, J. Ma, J. A. Tenreiro Machado, and G. Stepan (Springer, Cham, 2021), 75–85.

[42] S. J. D. D'Alessio, C. J. M. P. Seth, and J. P. Pascal, The effects of variable fluid properties on thin film stability, Phys. Fluids **26**, 122105 (2014).

[43] S. Chattopadhyay, P. Boragunde, A. K. Gaonkar, A. K. Barua, and A. Mukhopadhyay, Falling liquid films on a slippery substrate with variable fluid properties, Int. J. Non-Lin. Mech. **147**, 104200 (2022).

[44] S. V. Alekseenko, V. E. Nakoryakov, and B. G. Pokusaev, *Wave Flow of Liquid Films* (Begell House, New York, 1994).

[45] S. W. Joo, S. H. Davis, and S. G. Bankoff, Long-wave instabilities of heated falling films: Two-dimensional theory of uniform layers, J. Fluid Mech. **230**, 117 (1991).

[46] A. Mukhopadhyay and S. Chattopadhyay, Long wave instability of thin film flowing down an inclined plane with linear variation of thermophysical properties for very small Biot number, Int. J. Non-Lin. Mech. **100**, 20 (2018).

[47] A. Mukhopadhyay, S. Chattopadhyay, and A. K. Barua, Stability of thin film flowing down the outer surface of a rotating non-uniformly heated vertical cylinder, Nonlin. Dynam. **100**, 1143 (2020).

[48] S. Chattopadhyay, A. Mukhopadhyay, A. K. Barua, and A. K. Gaonkar, Thermocapillary instability on a film falling down a non-uniformly heated slippery incline, Int. J. Non-Lin. Mech. **133**, 103718 (2021).

[49] S. Chattopadhyay and A. S. Desai, Dynamics and stability of weakly viscoelastic film flowing down a uniformly heated slippery incline, Phys. Rev. Fluids **7**, 064007 (2022).

[50] S. Chattopadhyay, A. S. Desai, A. K. Gaonkar, A. K. Barua, and A. Mukhopadhyay, Weakly viscoelastic film on a slippery slope, Phys. Fluids **33**, 112107 (2021).

[51] Z. Ding and T. N. Wong, Falling liquid films on a slippery substrate with Marangoni effects, Int. J. Heat Mass Transf. **90**, 689 (2015).

[52] S. Chattopadhyay and A. Mukhopadhyay, Weakly viscoelastic film flowing down a rotating inclined plane, Phys. Fluids **34**, 012115 (2022).

[53] P. W. Carpenter and A. D. Garrad, The hydrodynamic stability of flow over Kramer-type compliant surfaces. Part 1. Tollmien-Schlichting instabilities, J. Fluid Mech. **155**, 465 (1985).

[54] P. W. Carpenter and A. D. Garrad, The hydrodynamic stability of flow over Kramer-type compliant surfaces. Part 2. Flow-induced surface instabilities, J. Fluid Mech. **170**, 199 (1986).

[55] A. S. Brown, Compliant substrate technology: Status and prospects, J. Vacuum Sci. Technol. B: Microelectr. Nanomet. Struct. Process. Meas. Phenom. **16**, 2308 (1998).